琉球大学学術リポジトリ

Variations of Field of Viscous Stress around Diapir Calculated by the Finite Element Method

メタデータ	言語: 出版者: 琉球大学理学部 公開日: 2008-03-27 キーワード (Ja): キーワード (En): 作成者: Hayashi, Daigoro, 林, 大五郎 メールアドレス: 所属:
URL	http://hdl.handle.net/20.500.12000/2629

Variations of Field of Viscous Stress around Diapir Calculated by the Finite Element Method

Daigoro HAYASHI*

Introduction

The writer has already presented a theory and finite element formulation of viscous fluid (Hayashi, 1975,1979), and applied it to the rise of diapir of migmatite to study a change of its form, rising velocity and surface uplift (Hayashi and Kizaki, 1979). Although main results for movement of the diapir were described in the latter paper, stress distributions were not done. The stress distribution around and within the diapir is discussed in the present paper. Calculations are performed by using FACOM 230-75 computer of Hokkaido University Computing Center.

Models

Models of stress analysis are the same as those were used by the writer's previous work (Hayashi and Kizaki, 1979), i.e. single-body model A, model B and the plural-bodies model C. These models are illustrated in Fig.1 and briefly explained as; single circular-shaped migmatite body with 8 km diameter lies at 10 km depth below the earth's surface with 10^{21} poises viscosity in model A, and with 10^{20} poises in model B. Four circular bodies of migmatite with 10^{19} poises viscosity lie at 5 km below surface in model C. Physical properties used in these models are summarized on Table 1. Initial boundary conditions and partitions of them are illustrated in Figs.2 and 3. The total numbers of elements and of nodal points of both the models A and B are 196 and 117, respectively. Those of model C are 148 and 90, respectively. All the models were calculated to obtain their deformed shapes and undulations of the earth's surface each 10, 20 and 30 Ma. Using the resultant coordinate of nodal points of each deformed model, viscous stress distributions are defined every 10 Ma by the FEM viscous stress computer program.

Process of Computation

Firstly, a suitable diapir, e.g. model A, B or C, is set up, then input data and band width of stiffness matrix are defined. Nextly, program is debugged and at the same time core memory and CPU-time of the program are estimated approximately. Calculations of viscous flow of diapir are performed to obtain the coordinates of displaced nodal points. Then, distributions of viscous principal stress are obtained by calculating the coordinates. The process is summarized on Table 2.

Received : April 30, 1980

* Department of Marine Sciences, Ryukyu University

Results and Discussion

Viscous principal stresses for the models A, B and C are all compressive and their distributions are shown in Figs. 4, 5 and 6, respectively. Referring to these figures, difference of viscosity between the models A and B does not affect significantly to absolute value of principal stresses and their principal directions.

Distributions of elastic principal stress of the models A, B and C are shown in Figs. 7, 8 and 9, respectively.

Physical constants used in the elastic analysis are given in Table 3. All elastic stresses are also compressive. Then, both the distributions of viscous and elastic stresses are compared with together to clarify a character of the distribution of viscous stress. It is obvious that the viscous ntress is extremely different from the elastic stress within upper half of each model, that is, vertically directed elastic principal stress (σ_2) is much larger than its laterally directed one (σ_1) where σ_1 is larger than σ_2 algebraically. Difference between σ_2 and σ_1 attains to about 80 percent of σ_2 in maximum. On the contrary, viscous stress is nearly hydrostatic, i. e. its σ_1 and σ_2 are almost identical.

It is the most important result of the stress analysis that viscous principal stress *around* the diapir has a tendency to range parallel with diapir-crust boundary. There are gneissosities parallel to the shape of the real migmatite body, e. g. the Oshirabetsu migmatite dome in the Hidaka metamorphic zone, Japan (Hayashi and Kizaki, 1972, 1979). On the contrary, that *within* diapir has not such a tendency. That is, the directions of viscous principal stress within crust around diapir connect closely with the orientations of foliation of gneiss around the diapir. In elastic models, such phenomenon does not appear as shown in the distributions of elastic stress and the writer's previous study (Hayashi and Kizaki, 1972).

Finally, magnitude of viscous principal stress is a little larger than that of elastic stress during rise of the present diapir models, though elastic constants are independent to viscous properties.

Mode of Computation

phenomenon; diapirism of migmatite
mechanism; dead load due to gravity
dimension; plane strain-rate
modelling material; incompressive Newtonian fluid without inertia term
method; FEM
species of computer; FACOM 230-75
used time; 7 min 18 sec (CPU-time except the time used for deformation of viscous flow)

Table 1 Physical contants used in the viscous stress analysis. η:viscosity ρ:density

model	rock	η(poises)	ρ(g/cm^3)
A	migmatite	10^{21}	2.76
	crust	10^{22}	3.04
B	migmatite	10^{20}	2.76
	crust	10^{22}	3.04
C	migmatite	10^{19}	2.76
	crust	10^{21}	3.04

Table 2 Process of computation

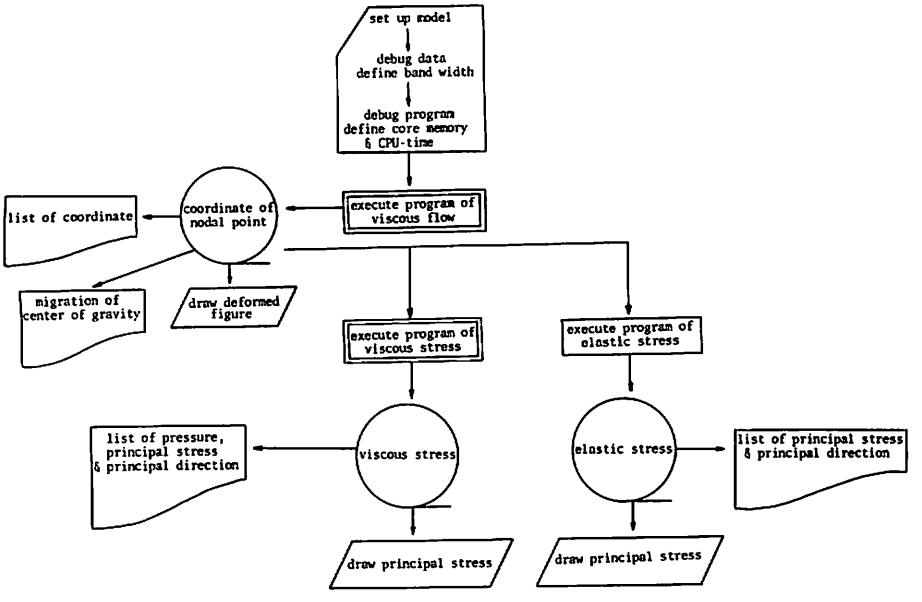

Table 3 Physical constants used in the elastic stress analysis, which are common in all models. E:Young's modulus ν:Poisson's ratio

rock	E(kb)	ν	ρ(g/cm^3)
migmatite	176	0.36	2.76
crust	304	0.40	3.04

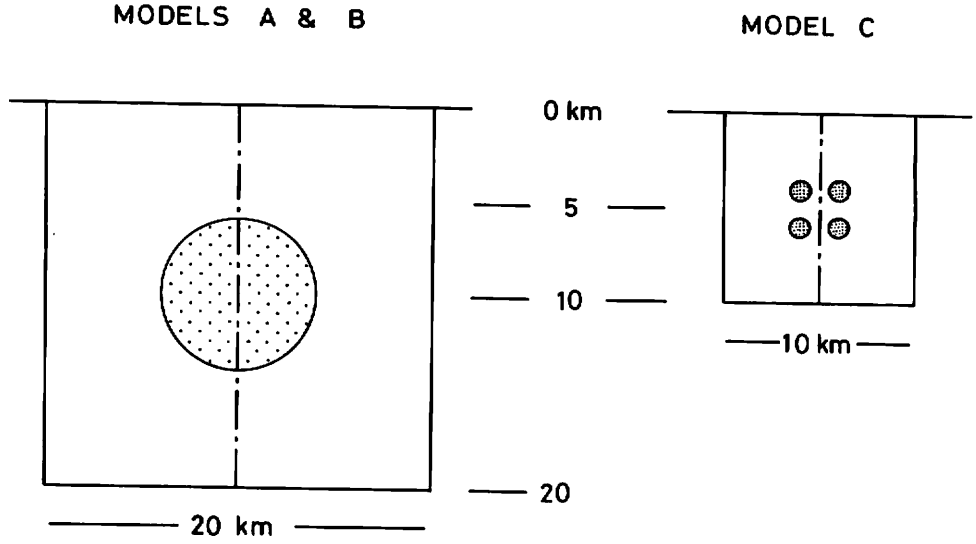

Fig.1 Single-body models A and B, and plural-bodies model C. Dotted area means migmatite body.

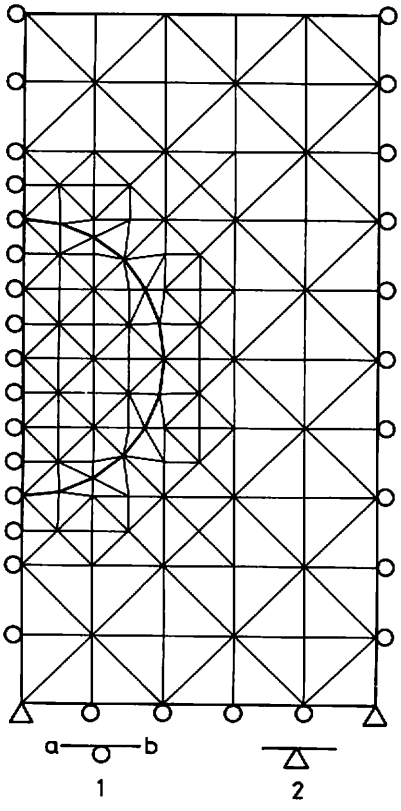

Fig.2 Initial boundary condition and partition in models A and B. 1=free along ab, 2=perfectly restricted.

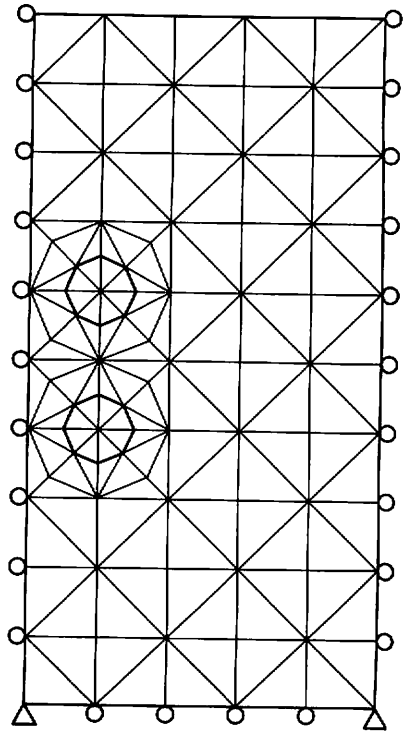

Fig.3 Initial boundary condition and partition in model C.

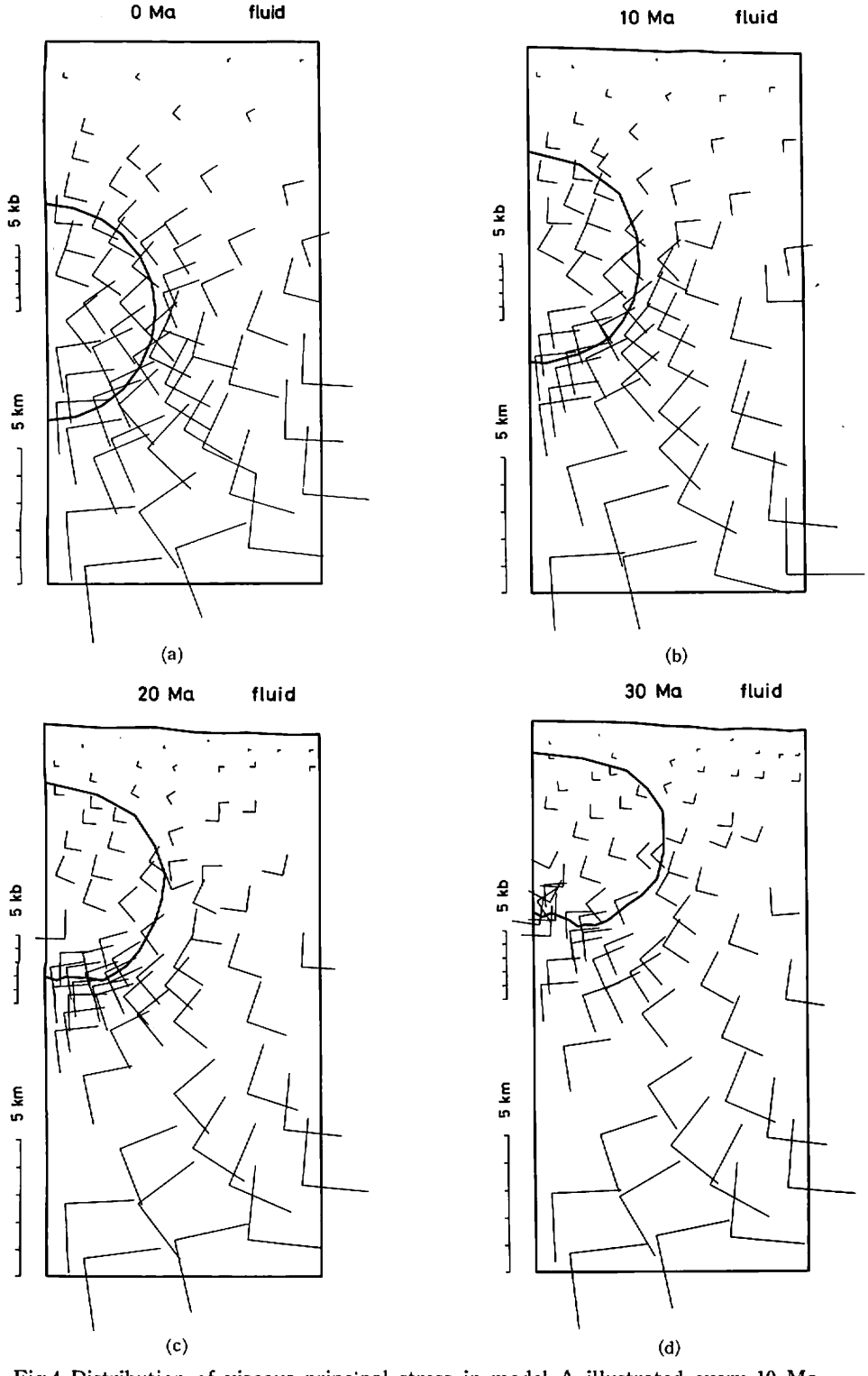

Fig.4 Distribution of viscous principal stress in model A illustrated every 10 Ma. All stresses are compressive. Ma=10^6 years

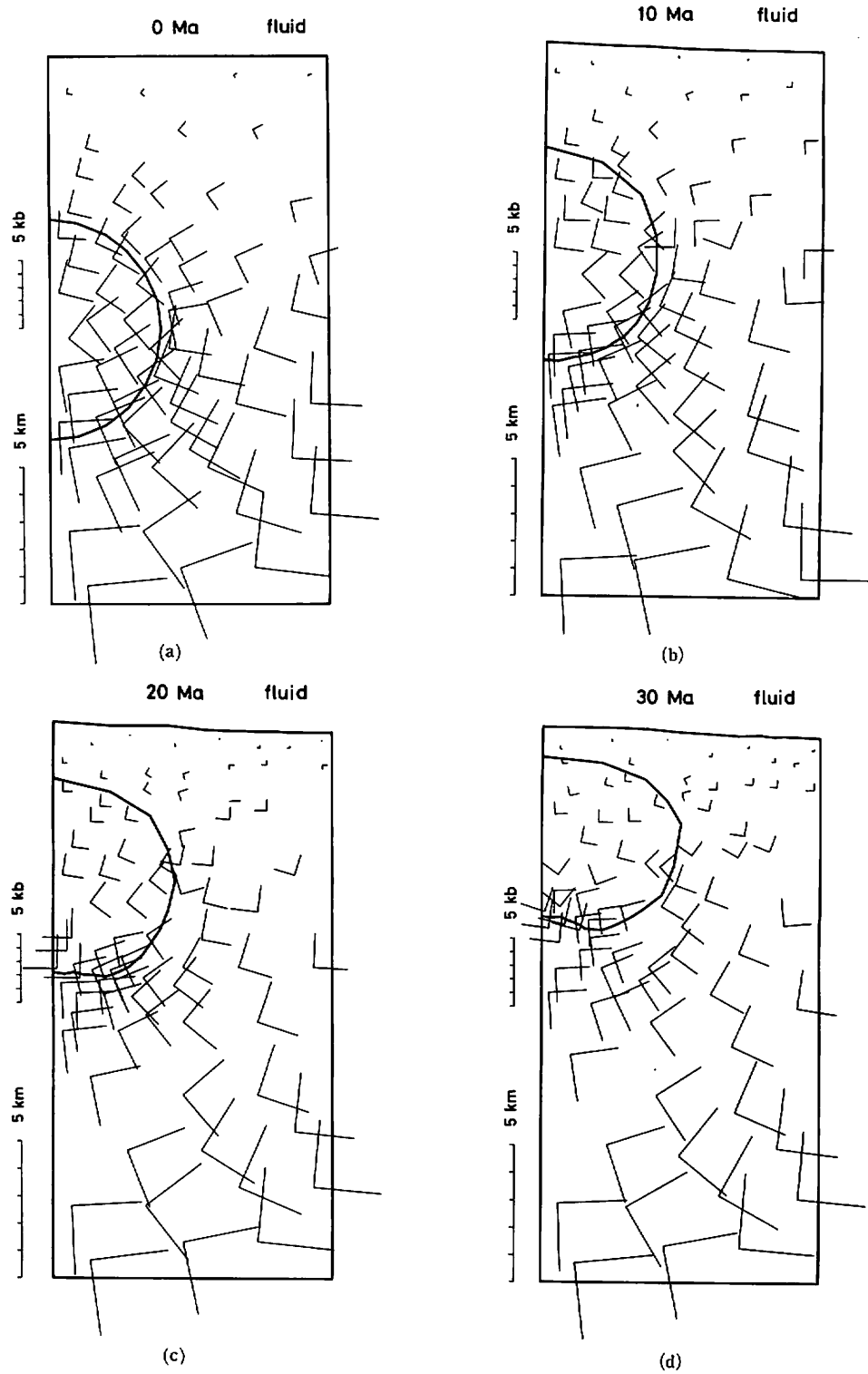

Fig.5 Distribution of viscous principal stress in model B illustrated every 10 Ma. All stresses are compressive.

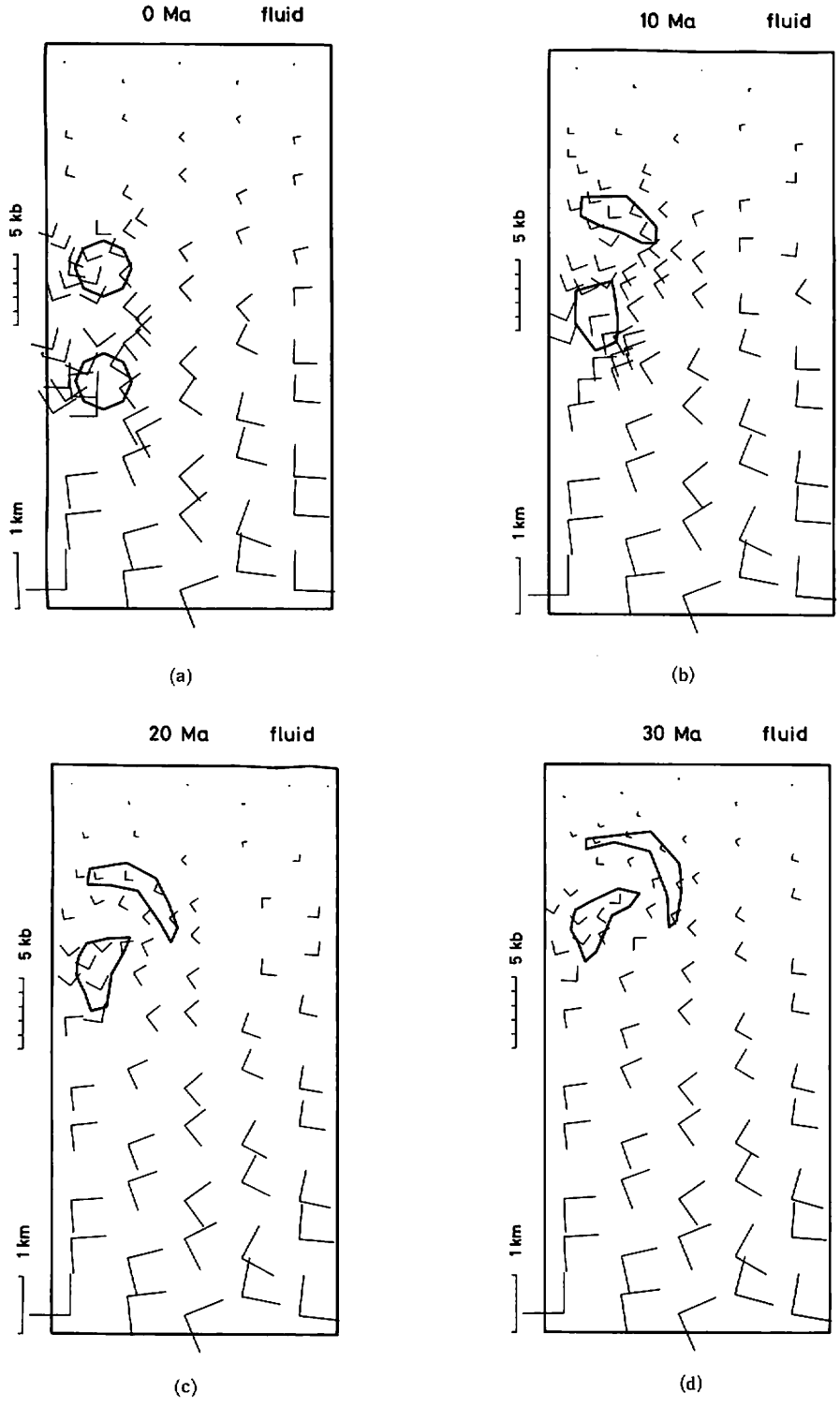

Fig.6 Distribution of viscous principal stress in model C illustrated every 10 Ma. All stresses are compressive.

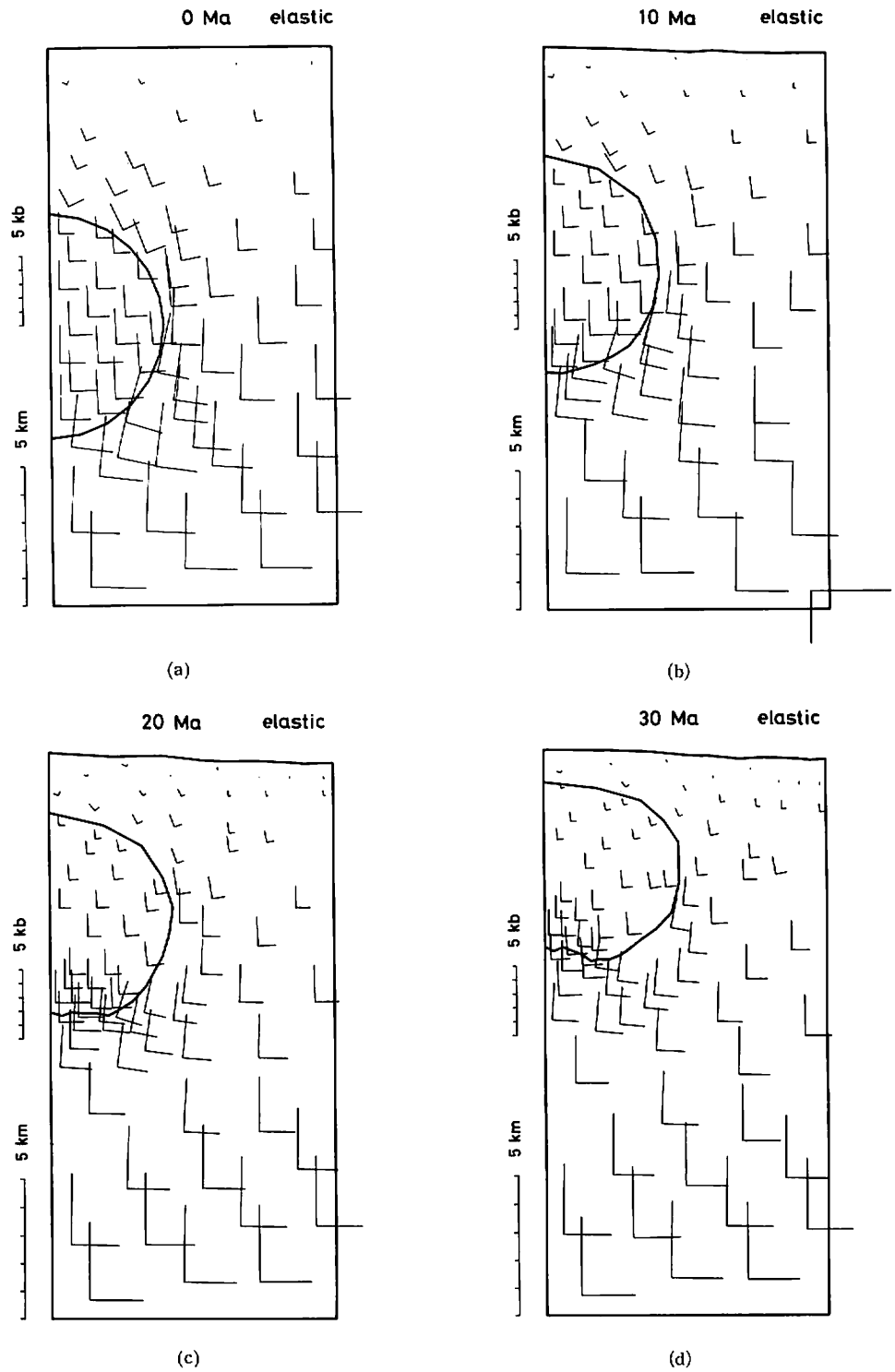

Fig.7 Distribution of elastic principal stress in model A illustrated every 10 Ma. All stresses are compressive.

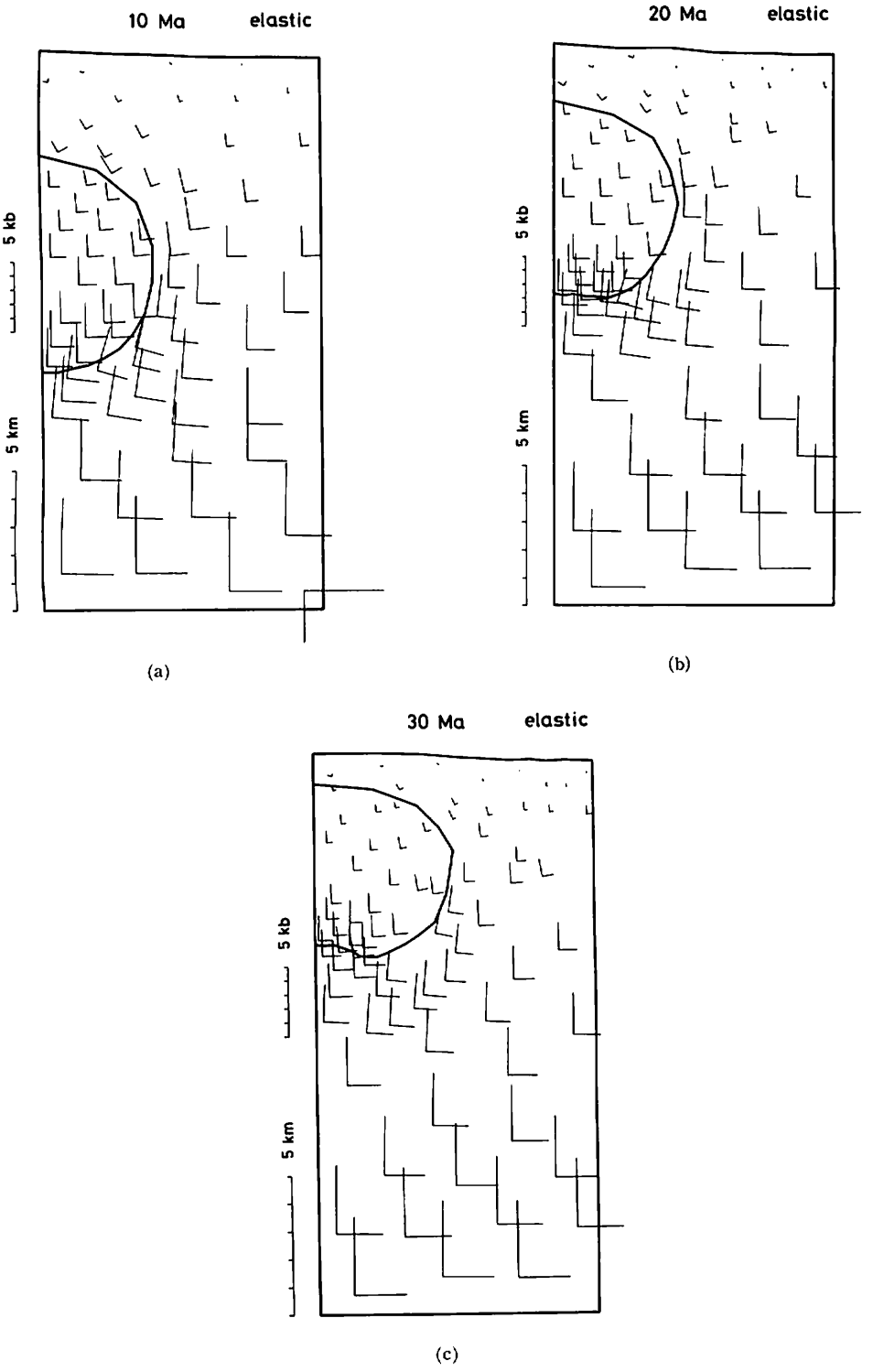

Fig.8 Distribution of elastic principal stress in model B illustrated every 10 Ma. All stresses are compressive. Stress figure at 0 Ma in the model is identical to Fig.7a.

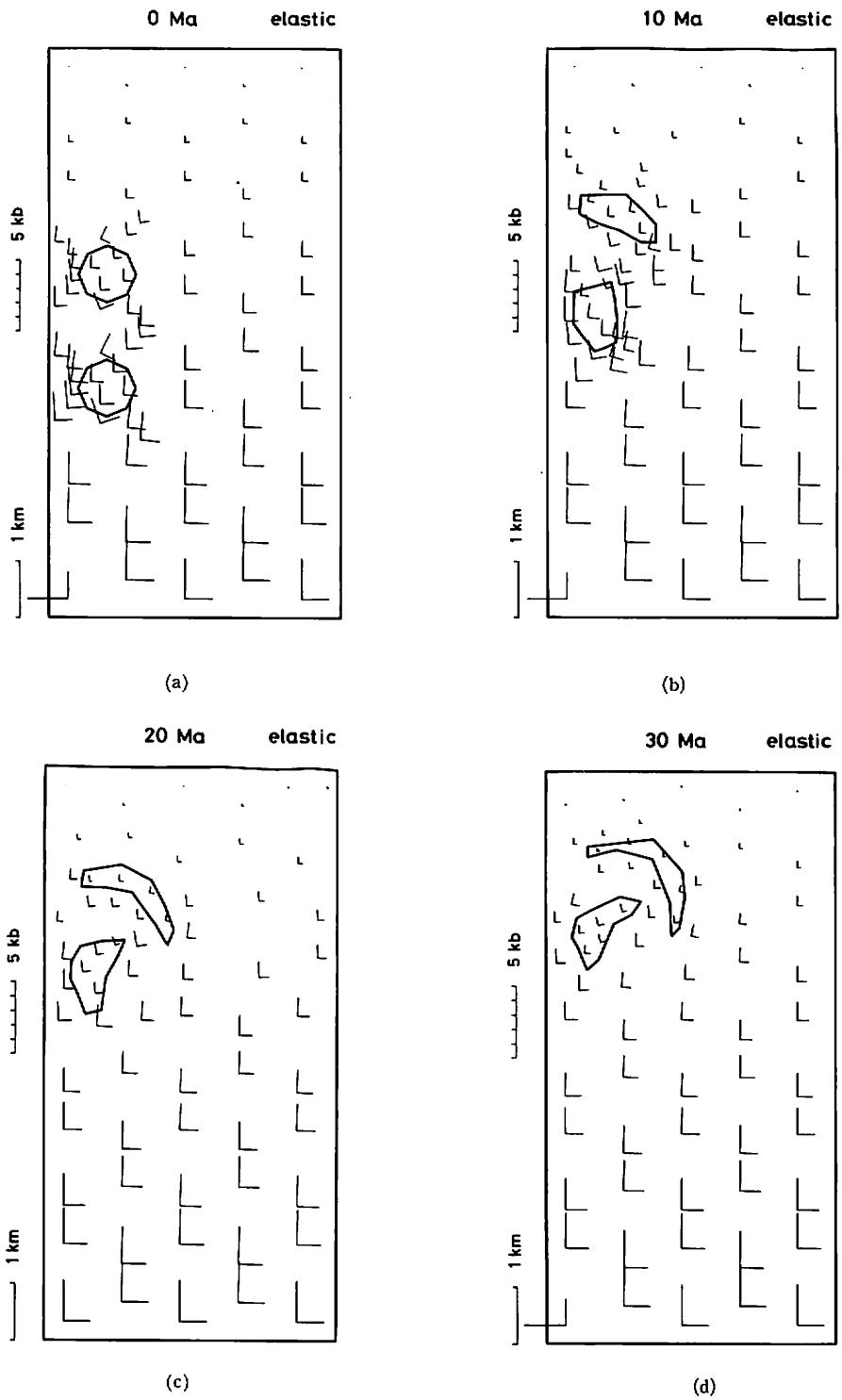

Fig.9 Distribution of elastic principal stress in model C illustrated every 10 Ma. All stresses are compressive.

References

Hayashi, D., 1975.Rising of a granitic mass as an incompressible Newtonian fluid. J. Geol. Soc. Jpn., **81**:769-782. (in Japanese with English abstract)

Hayashi, D., 1979. Finite element formulation of viscous fluid based on a variational principle. Bull. Coll. Sci. Ryukyu Univ., no. 28 : 119-130.

Hayashi, D. and Kizaki, K., 1972. Numerical analysis on migmatite dome with special reference to finite element method.J.Geol. Soc.Jpn., **78**:677-686.

Hayashi,D. and Kizaki,K., 1979. Numerical experiments of migmatite rise based on continuum dynamics. Tectonophysics, **60**:61-76.